

Short-Channel Field Effect Transistors with 9-Atom and 13-Atom wide Graphene Nanoribbons

*Juan Pablo Llinas¹, Andrew Fairbrother², Gabriela Barin², Pascal Ruffieux², Wu Shi⁴,
Kyunghoon Lee¹, Byung Yong Choi^{1,3}, Rohit Braganza¹, Nicholas Kau⁴, Wonwoo Choi⁴, Chen
Chen⁴, Zahra Pedramrazi⁴, Tim Dumlaff⁶, Akimitsu Narita⁷, Xinliang Feng⁶, Klaus Müllen⁷,
Felix Fischer⁵, Alex Zettl⁴, Michael Crommie⁴, Roman Fasel², Jeffrey Bokor^{1*}*

¹Dept. of Electrical Engineering and Computer Sciences, UC Berkeley, Berkeley, CA, USA

²Empa, Swiss Federal Laboratories for Materials Science and Technology, Dübendorf, CH

³Flash PA Team, Semiconductor Memory Business, Samsung Electronics Co. Ltd., Korea

⁴Dept. of Physics, UC Berkeley, Berkeley, CA, USA

⁵Dept. of Chemistry, UC Berkeley, Berkeley, CA, USA

⁶Center for Advancing Electronics Dresden, TU Dresden, Dresden, DE

⁷Max Planck Institute for Polymer Research, Mainz, DE

ABSTRACT: Graphene nanoribbons (GNRs) with armchair edges and <2 nm width are semiconducting and have great potential as a 1D channel material for ultra-scaled logic transistors. We demonstrate field effect transistors with channel lengths <20 nm fabricated with single atomically smooth graphene nanoribbon channels. These devices exhibit on-off ratios of 10^2 to 10^5 and showed a Schottky barrier limited on-current of up to 100 nA at -1 V drain bias. Using an ionic liquid gate dielectric, the on-state performance of devices with 9-atom wide armchair GNRs was improved to 300 nA at 0.2 V drain bias.

As field effect transistors (FETs) for advanced digital logic circuits approach the sub-10nm gate length regime, the device structure and channel material must account for multiple mechanisms that increase off-state leakage^{1,2}. An ultra-thin body and large band gap (>1 eV) can be used to successfully implement transistors at these length scales. Carbon nanotubes (CNTs) or graphene nanoribbons (GNRs) have been theoretically shown to have favorable properties for this purpose¹. High-performance scaled CNTFETs have been successfully demonstrated down to 9 nm gate lengths³, but both the on-state and off-state performance is strongly dependent on the nanotube chirality. Current CNT chirality sorting techniques do not yield sufficient purity for very large scale integration (VLSI)⁴. As an alternative, ultra-narrow graphene nanoribbons (GNRs) have the desired thin body to allow for gate control and band gaps as large as 2.35 eV or more which suppress band to band tunneling at channel lengths <7 nm¹.

The electronic, optical, and magnetic properties of graphene nanoribbons can be engineered by varying their width and edge structure⁵⁻¹⁰. However, traditional methods to pattern GNRs, such as unzipping carbon nanotubes or lithographically defining GNRs from bulk graphene, yield GNRs with rough edges that degrade electronic transport¹¹. Recent experiments have

demonstrated bottom-up chemical synthesis of graphene nanoribbons with atomically smooth and well-defined edges¹²⁻¹⁵, enabling the study of charge transport in these structures with definite electronic structure. The edge structure and width of the GNRs can be controlled by varying the structure of the monomer used in the polymerization step of the synthesis. The GNRs grown by this synthesis method have uniform width and atomically defined edges, thus making all the GNRs electronically identical. For instance, if the synthesis is carried out with a monomer designed to make 7-atom wide GNRs with armchair edges, all the resulting GNRs would be semiconducting with a predicted band gap of 3.8 eV¹². This level of homogeneity in electronic structure has yet to be achieved in CNTs, which is one of the significant limiting factors of the integration of CNTFETs into logic processors⁴.

Field-effect transistors (FETs) fabricated with 7 atom wide GNRs (7AGNRs) and Pd contacts have shown low driving current of 1 nA for 1 V drain bias due to the large contact resistance caused by the Schottky barrier at GNR-Pd interface¹⁶. This is not surprising considering the large band gap of 7AGNRs of 3.8 eV. The band gap of GNRs that are several nm wide decreases with increasing width. However, for GNRs that are <2 nm wide, the band gap relation to the width depends strongly on the type of armchair edge termination⁸. There are three different possible armchair edge terminations. As a result, the band gap trend splits into three families, $N = 3p, 3p + 1, 3p + 2$, where N is the width of the GNR in number of atoms and p is an integer, 0, 1, 2, ... Atomistic calculations performed by Yang et. al.⁸ show that GNRs with widths less than 2 nm in the $3p + 1$ family tend to have the smallest band gaps (e.g. the 11-atom wide GNR has a band gap of 0.9 eV). On the other hand, GNRs in the $3p + 2$ family tend to have the largest band gaps: 2.35 eV for the 13-atom wide GNR or 3.8 eV for the 7-atom wide GNR. The trend in the band gap of GNRs in the $3p$ family tends to fall in between the $3p + 1$ and $3p + 2$ families. Since

the height of the Schottky barrier at the contact depends roughly linearly with band gap, we employed bottom up synthesis of 9-atom¹⁷ and 13-atom¹⁵ wide GNRs – with predicted band gaps of 2.1 and 2.35 eV, respectively – to improve the on-state performance of GNRFETs. FETs with 9 and 13 atom wide GNRs are demonstrated with 100 nA of on-current and on-off ratios $> 10^3$, showing a two order magnitude improvement in on-current over the 7AGNRFET for the same bias.

We fabricated field effect transistors using 9-atom and 13-atom wide armchair GNRs (9AGNRs and 13AGNRs, respectively). The 9AGNRs and 13AGNRs are synthesized similarly, differing only in type of monomer used and process variables such as the temperatures of sublimation, polymerization, and cyclodehydrogenation. The desired monomer is evaporated onto an Au(111) surface of a thin-film Au on mica substrate under ultra-high vacuum and heated until it polymerizes on the surface. Heating the substrate further causes individual polymers to planarize into graphene nanoribbons (cyclodehydrogenation). The quality of the GNRs are then verified by scanning tunneling microscope (STM)^{12,15} imaging as shown in Fig. 1. Other studies using non-contact atomic force microscopy have shown the definite atomic structure along the ribbon¹⁸.

Fabrication of GNRFETs requires the transfer of GNRs from the Au growth surface to an insulating surface. We floated the Au/mica substrate in 38% HCl, which caused the mica to delaminate with the Au film remaining on the surface of the acid¹³. We picked up the floating gold film with a 50 nm SiO₂ / p++ Si substrate. Subsequent gold etching in KI/I₂ yields isolated GNRs on the SiO₂ surface. Since the GNRs are only tens of nanometers long, we used electron beam lithography and lift-off processing to pattern 10 nm thick, 100 nm wide Pd electrodes with 10-20 nm channel length. The final device structure is illustrated in Fig 1. Using the same

fabrication methods, we made two different types of samples: one with 9AGNRs and one with 13AGNRs. Finally, we characterized the electrical transport properties of individual devices.

For the 9AGNR and 13AGNR chips, we patterned ~300 pairs of electrodes in the transferred GNR area. To determine whether the gap between electrodes is bridged by one or more GNRs, each defined channel was biased and tested for gate modulation in the current. Of the 300 devices, 28 devices and 29 devices were successfully fabricated for 9AGNR and 13AGNRs, respectively. This sort of device yield indicates that most of the devices found only have one GNR in the channel as demonstrated by Fig. S1.

As shown in Fig. 2, both the 9AGNRFETs and the 13AGNRFETs showed similar performance and behavior due to their similar band gap^{8,15,17}. All the devices behave as semiconducting p-type Schottky barrier devices with a positive threshold gate voltage in ambient conditions with on-off ratios in the range of 10^2 to 10^5 . However, when the devices are measured in vacuum at room temperature, the threshold voltage shifts towards 0 V as shown in Fig. 2. This effect has been observed in CNTFETs and is attributed to the charge trapping of water molecules in the vicinity of the CNT causing hysteretic effects on the gate control^{19,20}. Spatial fluctuations in these charge impurities and the variation in channel length are likely contributing the variation in on-off ratio in our devices due to the rather thick gate electrode for such a small channel geometry. The on-current varies in our devices from 10s of nA to 100s nA, as shown in the commutative distribution function (CDF) of on-current in Fig. 2(b), which we attribute to variation in channel length, contact overlap length, and the aforementioned variance in gate control. Since we expect GNRFETs with high carrier transparency contacts to conduct more than 1 μ A at this bias (as opposed to ~100 nA in our highest current devices)⁹, we measured some of the devices in vacuum at various temperatures to study the transport mechanism at the contacts.

We observed rectifying behavior in the I_d – V_d characteristics of the devices as shown in Fig. 3, indicating the presence of large Schottky barriers at the Pd-GNR interface. A large Schottky barrier is expected to dominate transport at the contacts with GNRs of band gaps of the order of 2 eV. To determine the contributions of thermionic vs tunneling current at Pd-GNR interface, we measured the devices in vacuum at 77 K, 140 K, 210 K, and 300 K. As shown in Fig. 3 and Fig. 4, there is no significant change in conduction at these different temperatures for either 13AGNRFETs or 9AGNRFETs. This weak temperature dependence in conduction indicates the occurrence of tunneling through the barriers as opposed to thermionic emission over the barriers at the contacts. Furthermore, the ambipolar behavior observed at low temperatures is only realistically possible with tunneling contacts, since thermally activated current is suppressed for electrons. Tunneling contacts with weak temperature dependence have been observed for CNTFETs and other low-dimensional materials and verified via simulations^{21–23}. We conclude that the improvement in on-state performance over 7AGNRFETs is largely due to the smaller hole barrier height at the contacts. Therefore, to further improve the on-state performance, wider GNR's with smaller band gaps could be used to reduce the height and width of the Schottky barrier. Alternatively, finding a metal with a Fermi level that aligns closer to the GNR's valence band (or conduction band in case of n-type Schottky barrier transistors) would yield similar results while maintaining low offstate current.

Since the transmission probability of carriers at the contacts depends on the width of the Schottky barrier, the current can be improved by increasing the magnitude of the electric field at the Pd-GNR interface. The barrier widths for both holes and electrons can be thinned efficiently by using an ionic liquid (IL) gate dielectric, improving both electron and hole conduction in a device²⁴. We used an IL dielectric (DEME-TFSI) to improve the electrostatic coupling between

the gate electrode and the GNR channel, increase the field at the Pd-GNR interface, and improve both hole and electron conduction across the contacts. The $I_d - V_g$ behavior of a 9AGNRFET with IL gating is shown in Fig. 5. This device shows clear ambipolar behavior and a hole current of around 200 nA at 0.2 V drain bias (as opposed to 100 nA at -1 V for the 50 nm SiO₂ dielectric device). Due to the high gate efficiency of the ionic liquid, the transistor switches at smaller gate voltages. This result demonstrates that lowering and thinning of the Schottky barrier by contact engineering can significantly improve the current.

We demonstrated that both 9AGNRFETs and 13AGNRFETs showed significant performance improvement over the previously reported 7AGNRFETs and exhibited no significant temperature dependence in their behavior. This work highlights progress towards high-performance GNR devices for logic applications. Further work is needed to improve the contact resistance of GNRFETs by lowering the Schottky barrier and to reduce device-to-device variability.

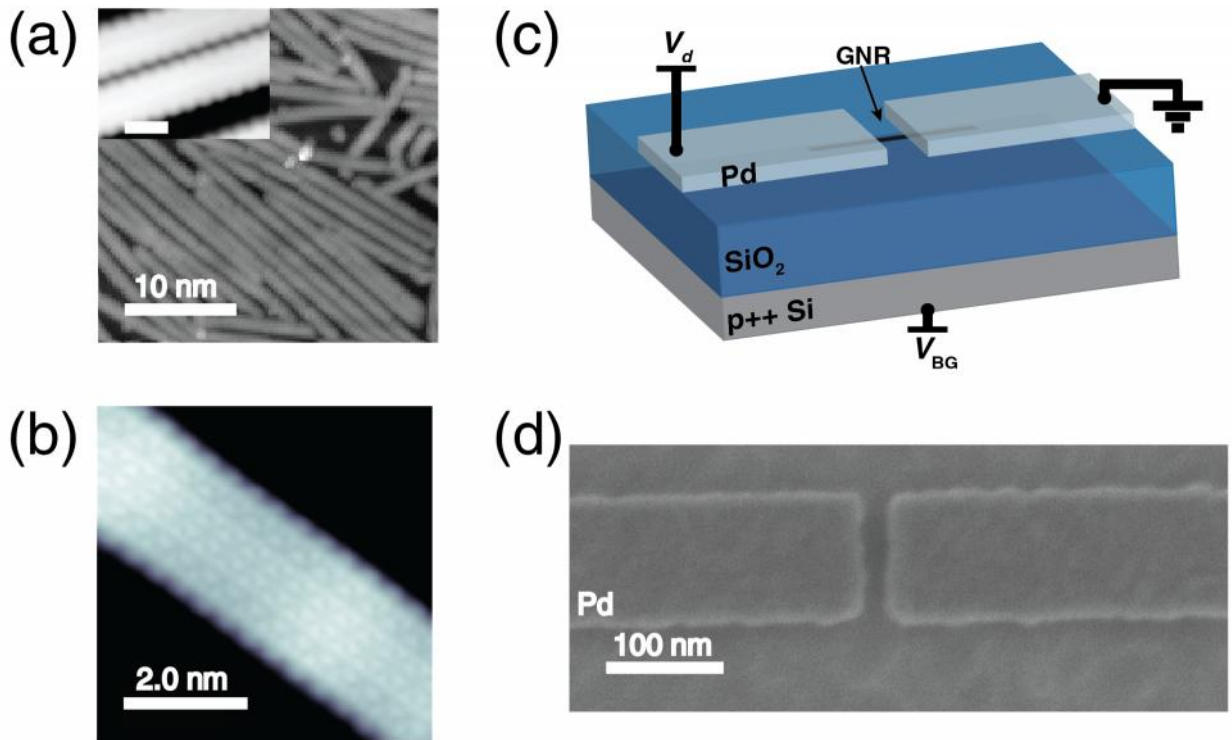


Figure 1. (a) STM image of synthesized 9AGNR on Au ($V_s = 1$ V, $I_t = 0.3$ nA). Inset: High resolution STM image of 9AGNR on Au ($V_s = 1$ V, $I_t = 0.5$ nA) with a scale bar of 1 nm (b) High resolution STM image of 13AGNR on Au ($V_s = -0.7$ V, $I_t = 7.02$ nA). (c) Schematic of the fabricated GNRFETs with 50 nm SiO_2 back gate. (d) Scanning electron micrograph of the fabricated Pd source-drain electrodes.

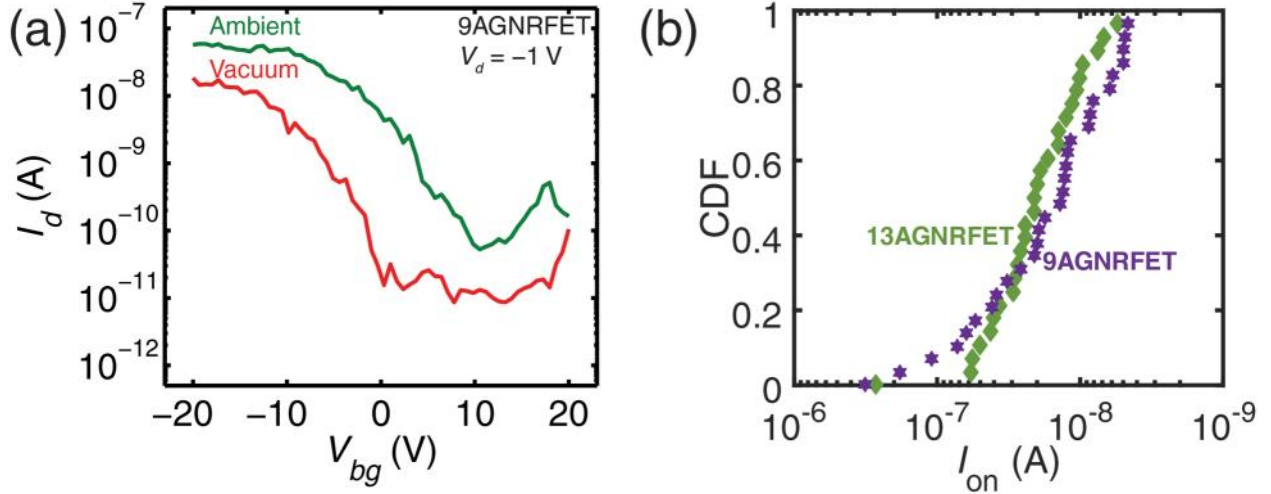


Figure 2. (a) I-V characteristics of an 9AGNRFET in vacuum and in ambient conditions. Water is desorbed in vacuum which causes the threshold voltage to shift towards 0 V. (b) CDF showing the fraction of 9AGNRFETs and 13AGNRFETs with I_{on} greater than the value on the horizontal axis. All devices were measured at $V_{bg} = -20$ V and $V_d = -0.6$ V in ambient conditions.

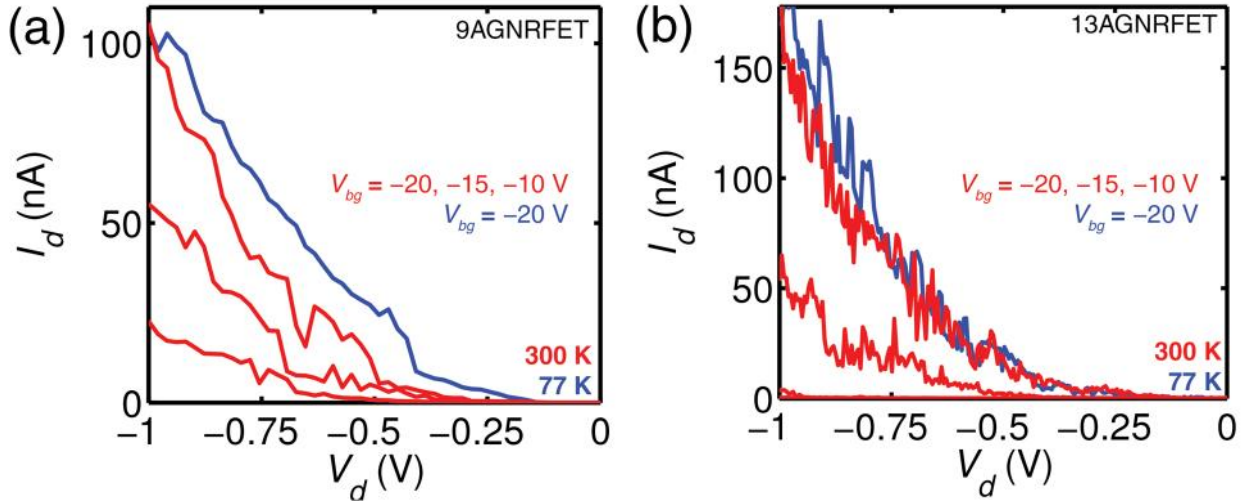


Figure 3. Temperature dependence of I_d - V_d characteristics of 9AGNRFET (a) and 13AGNRFET (b). The presence of a Schottky barrier is confirmed by non-linear current behavior at low drain bias and lack of current saturation at high drain bias.

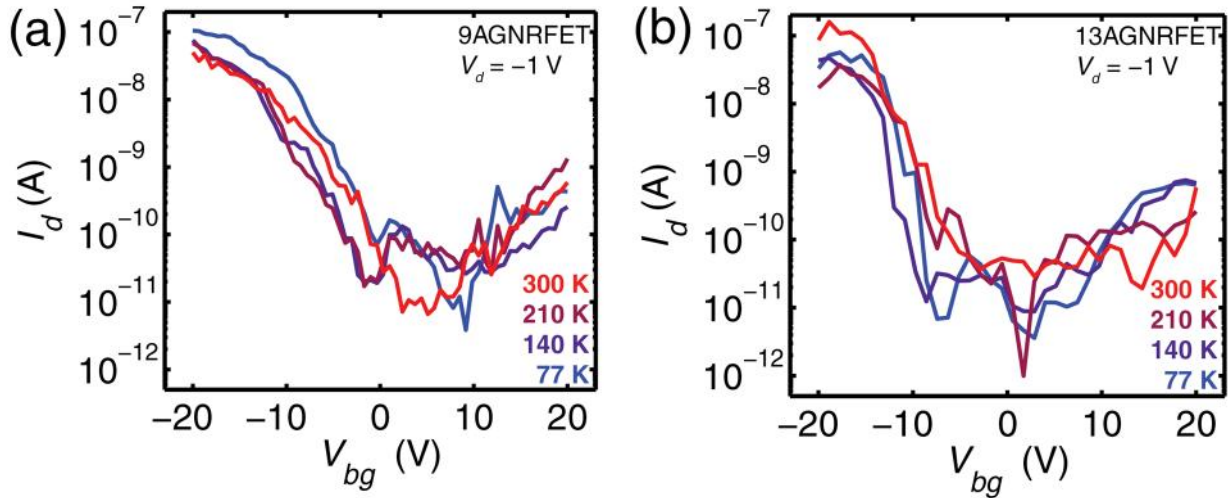


Figure 4. Temperature dependence of I_d - V_{bg} characteristics of (a) 9AGNRFET and (b) 13AGNRFET. The weak temperature dependence of the current indicates that tunneling through the Pd-GNR Schottky barriers is the main transport mechanism at the contacts.

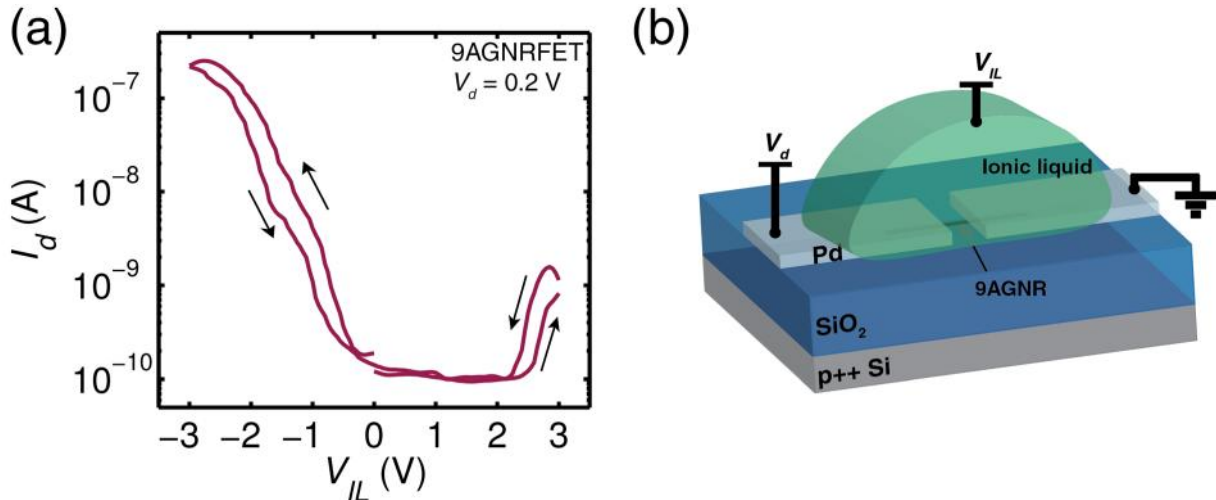


Figure 5. Ionic liquid gating of a 9AGNRFET with a V_{IL} sweep speed of 50 mV/s. (a) I_d - V_{IL} shows clear ambipolar behavior with a ~ 2 V off-state region. (b) Ionic liquid (DEME-TFSI) gate 9AGNRFET device schematic.

Supporting Information. Device fabrication steps, GNR growth, and statistical analysis of the number of GNRs in the channel.

Corresponding Author

*jbokor@eecs.berkeley.edu

ACKNOWLEDGMENT

This work was supported in part by the Office of Naval Research BRC program, DARPA, the U. S. Army Research Laboratory and the U. S. Army Research Office under contract/grant number W911NF-15-1-0237, and the Swiss National Science Foundation. Work at the Molecular Foundry was supported by the Office of Science, Office of Basic Energy Sciences, of the U.S. Department of Energy under Contract No. DE-AC02-05CH11231. J.P.L. is supported by the Berkeley Fellowship for Graduate Studies and by the NSF Graduate Fellowship Program.

REFERENCES

- (1) Luisier, M.; Lundstrom, M.; Antoniadis, D. A.; Bokor, J. In *Electron Devices Meeting (IEDM), 2011 IEEE International*; 2011; pp 11.2.1–11.2.4.
- (2) Ieong, M.; Doris, B.; Kedzierski, J.; Rim, K.; Yang, M. *Science* **2004**, *306* (5704), 2057–2060.
- (3) Franklin, A. D.; Luisier, M.; Han, S.-J.; Tulevski, G.; Breslin, C. M.; Gignac, L.; Lundstrom, M. S.; Haensch, W. *Nano Lett.* **2012**, *12* (2), 758–762.
- (4) Franklin, A. D. *Nature* **2013**, *498* (7455), 443–444.
- (5) Nakada, K.; Fujita, M.; Dresselhaus, G.; Dresselhaus, M. S. *Phys. Rev. B* **1996**, *54* (24), 17954–17961.
- (6) Han, M. Y.; Özyilmaz, B.; Zhang, Y.; Kim, P. *Phys. Rev. Lett.* **2007**, *98* (20), 206805.
- (7) Son, Y.-W.; Cohen, M. L.; Louie, S. G. *Nature* **2006**, *444* (7117), 347–349.
- (8) Yang, L.; Park, C.-H.; Son, Y.-W.; Cohen, M. L.; Louie, S. G. *Phys. Rev. Lett.* **2007**, *99* (18), 186801.
- (9) Liang, G.; Neophytou, N.; Nikonov, D. E.; Lundstrom, M. S. *IEEE Trans. Electron Devices* **2007**, *54* (4), 677–682.
- (10) Hsu, H.; Reichl, L. E. *Phys. Rev. B* **2007**, *76* (4), 045418.

- (11) Yoon, Y.; Guo, J. *Appl. Phys. Lett.* **2007**, *91* (7), 073103.
- (12) Cai, J.; Ruffieux, P.; Jaafar, R.; Bieri, M.; Braun, T.; Blankenburg, S.; Muoth, M.; Seitsonen, A. P.; Saleh, M.; Feng, X.; Müllen, K.; Fasel, R. *Nature* **2010**, *466* (7305), 470–473.
- (13) Cai, J.; Pignedoli, C. A.; Talirz, L.; Ruffieux, P.; Söde, H.; Liang, L.; Meunier, V.; Berger, R.; Li, R.; Feng, X.; Müllen, K.; Fasel, R. *Nat. Nanotechnol.* **2014**, *9*, 896–900
- (14) Chen, Y.-C.; Cao, T.; Chen, C.; Pedramrazi, Z.; Haberer, D.; Oteyza, D. G. de; Fischer, F. R.; Louie, S. G.; Crommie, M. F. *Nat. Nanotechnol.* **2015**, *10* (2), 156–160.
- (15) Chen, Y.-C.; de Oteyza, D. G.; Pedramrazi, Z.; Chen, C.; Fischer, F. R.; Crommie, M. F. *ACS Nano* **2013**, *7* (7), 6123–6128.
- (16) Bennett, P. B.; Pedramrazi, Z.; Madani, A.; Chen, Y.-C.; Oteyza, D. G. de; Chen, C.; Fischer, F. R.; Crommie, M. F.; Bokor, J. *Appl. Phys. Lett.* **2013**, *103* (25), 253114.
- (17) Söde, H.; Talirz, L.; Sanchez-Valencia, J. R.; Wang, S.; Berger, R.; Dumslaff, T.; Narita, A.; Feng, X.; Müllen, K.; Meunier, V.; Fasel, R.; Ruffieux, P. *in preparation*.
- (18) van der Lit, J.; Boneschanscher, M. P.; Vanmaekelbergh, D.; Ijäs, M.; Uppstu, A.; Ervasti, M.; Harju, A.; Liljeroth, P.; Swart, I. *Nat. Commun.* **2013**, *4*, 2023.
- (19) Kim, W.; Javey, A.; Vermesh, O.; Wang, Q.; Li, Y.; Dai, H. *Nano Lett.* **2003**, *3* (2), 193–198.
- (20) Franklin, A. D.; Tulevski, G. S.; Han, S.-J.; Shahrjerdi, D.; Cao, Q.; Chen, H.-Y.; Wong, H.-S. P.; Haensch, W. *ACS Nano* **2012**, *6* (2), 1109–1115.
- (21) Chen, Z.; Appenzeller, J.; Knoch, J.; Lin, Y.; Avouris, P. *Nano Lett.* **2005**, *5* (7), 1497–1502.
- (22) Appenzeller, J.; Radosavljević, M.; Knoch, J.; Avouris, P. *Phys. Rev. Lett.* **2004**, *92* (4), 048301.
- (23) Perebeinos, V.; Tersoff, J.; Haensch, W. *Phys. Rev. Lett.* **2013**, *111* (23), 236802.
- (24) Zhang, Y.; Ye, J.; Matsuhashi, Y.; Iwasa, Y. *Nano Lett.* **2012**, *12* (3), 1136–1140.

Supplemental Information

1. Methods

Preparation of target substrate

Using dry oxidation, 50 nm SiO₂ was grown on heavily doped 150 mm silicon wafers. Alignment markers and large pads for electrical probing were patterned using standard photolithography and lift-off of 3 nm Cr and 25 nm Pt. The wafer was then diced and individual chips were used for GNR transfer and further device processing.

13AGNR growth

13-AGNRs were synthesized using 10,10 -dibromo-9,9 -bianthracene (DBBA) building blocks. A thin film of Au(111) on mica was used as the substrate in this work. Standard Ar+ sputtering/annealing cycles were applied to prepare an atomically clean surface. A home-built Knudsen cell was used to sublime the DBBA molecular building blocks at 222 C onto the clean substrate held at room temperature. The sample was then slowly annealed stepwise to 340 C to fabricate 13AGNRs.

9AGNR growth

9AGNRs are synthesized from 3',6'-dibromo-1,1':2',1"-terphenyl precursor monomers (see Ref. 17 for details). First, the Au/mica substrate (200 nm Au; PHASIS, Geneva, Switzerland) is cleaned in ultra-high vacuum by two sputtering/annealing cycles : 1 kV Ar⁺ for ten minutes followed by a 470 °C anneal for ten minutes. Next, the monomer is sublimed onto the Au(111) surface at a temperature of 60-70 °C, with the substrate held at 180 °C. After 2 minutes of deposition (resulting

in approximately half monolayer coverage), the substrate temperature is increased to 200 °C for ten minutes to induce polymerization, followed by annealing at 410 °C for ten minutes in order to cyclodehydrogenate the polymers and form 9AGNRs.

Electron beam lithography

After the GNR transfer described in the main text, 950K MW PMMA was spun on the chips at 4krpm and followed by a 10 min bake at 180 C. ~300 source drain electrodes (100 nm wide, with gaps of 15-20 nm) were patterned using a JEOL 6300-FS 100 kV e-beam lithography system and subsequent developed in 3:1 IPA:MIBK at 5 C. 10 nm Pd was deposited using ebeam evaporation and lift-off was completed in Remover PG at 80 C.

Electrical characterization

Devices were first screened in ambient conditions using a cascade probe station and an Agilent B1500A parameter analyzer. Vacuum and variable temperature measurements were then performed in a Lakeshore probe station.

2. Extraction of number of GNRs in the channel

We used a Monte Carlo simulation to estimate the number of GNRs in our device channels based on our device yield. Assuming a uniform spatial distribution of GNRs, the simulation outputs an expected device yield and distribution of number of GNRs in the channel. The input parameters of the simulation were the GNR number density on the surface and GNR length. We varied these parameters to generate Fig. S1. With the experimentally obtained yield of ~10%, the percentage of devices with more than 1 GNR in the channel goes as high as 8% for higher surface density and 4% for low surface density. Out of the devices with multiple GNRs, an insignificant percentage

have more than 2 GNRs/channel. Thus, we estimate that only 1-3 devices out of ~30 fabricated devices have 2 GNRs in the channel. However, it is unclear whether these devices would account of the high tail end of the on-current distribution since both GNRs would have to have good contact length under the Pd contacts to improve conduction over a single GNR channel with a large contact length.

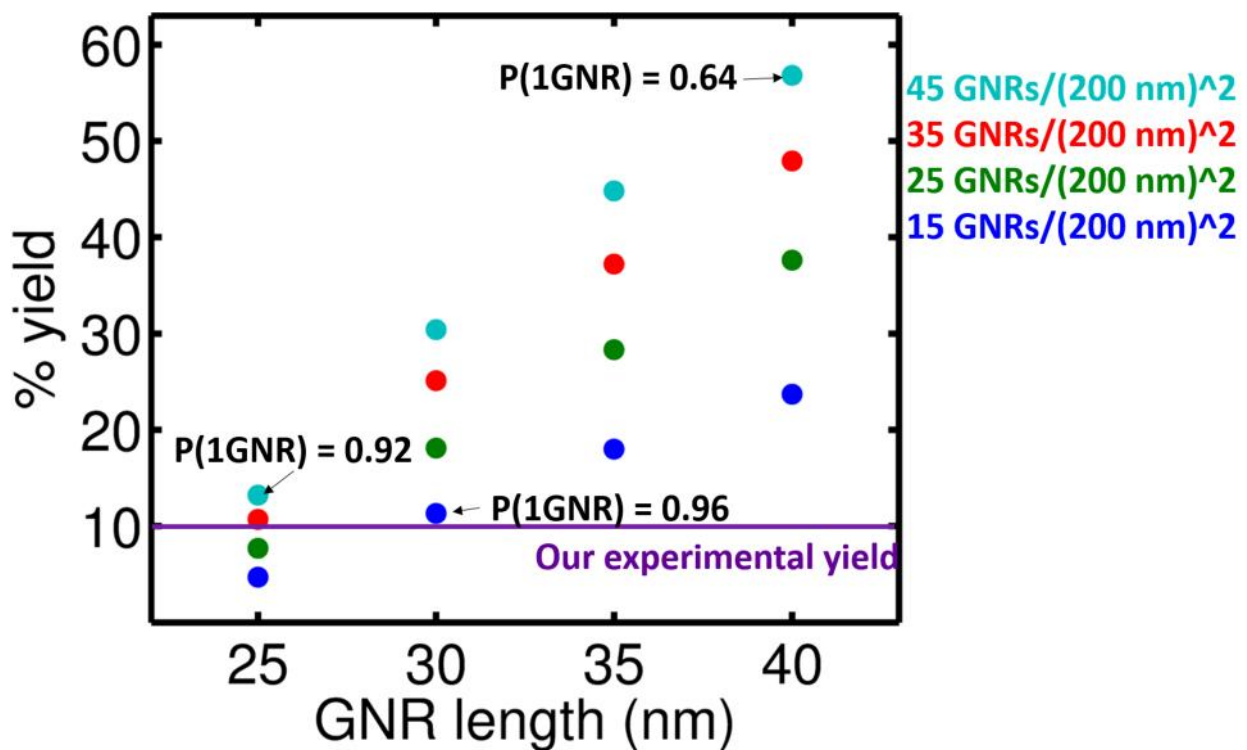


Figure S5. Simulated % yield of working devices as a function of GNR length and number density. The $P(1\text{GNR})$ values denote the probability of a yielded device to have a single GNR in the channel. With our ~10% experimental yield, we estimate that only 1-3 devices contain 2 GNRs in the channel.